East European Journal of Physics. **3**. 50–68 (2025)
DOI: 10.26565/2312-4334-2025-3-05 ISSN 2312-4334

COUPLED-CHANNELS ANALYSIS AND OPTICAL MODEL POTENTIAL EXTRACTION FOR DEUTERON SCATTERING FROM ^{6}Li TO ^{208}Pb

Waleed Saleh Alrayashi*
Science Department, Faculty of Education, Sana'a University, Sanna'a, Yemen
**Corresponding Author e-mail: walrayashi@su.edu.ye*
Received May 5, 2025; revised June 11, 2025; in final form June 16, 2025; accepted June 17, 2025

Deuteron-nucleus elastic and inelastic scattering from ^{6}Li to ^{208}Pb has been studied for incident energies ranging from 9.9 to 270 MeV. The main goal of this work is to study the effect of coupling the nuclear ground state to inelastic excitation channels on the energy dependence of optical model potential (OMP) parameters. Using the FRESCO and SFRESCO codes, we explicitly coupled the elastic channel to low-lying collective states and extracted OMP parameters through χ^2 minimization. The best-fit optical model parameters were obtained for elastic and inelastic angular distribution data. Our elastic and inelastic angular distribution fits show excellent agreement with the experimental data since more than one set of potential parameters can reproduce a given angular distribution data. When the ground state was coupled to the most important inelastic excitation channels the energy dependence of the OMP parameters was reduced. This is most obvious for optical model parameters whose value became almost constant when channel coupling was considered.

Keywords: *Coupled-Channel Reactions; Deuteron; Elastic scattering; Inelastic scattering; Optical model potential parameters; Differential cross section*

PACS: 24.10.Eq, 24.10.Ht, 25.45.De, 24.10.-i

1. INTRODUCTION

The study of nuclear interactions is extremely important, as it provides valuable information about the properties of nuclei. A nuclear interaction occurs when a projectile (particle or nucleus) interacts with a target nucleus. The study of nuclear particle scattering processes, such as deuteron-nucleus scattering, provides important tools for understanding the nature of fundamental nuclear interactions and determining the characteristics of the potential between the projectile and the target nucleus. Nuclei are complex composite particles composed of a large number of constituent particles. This makes constructing microscopic models of deuteron-nucleus interactions a challenging task, further complicated by the fact that we still do not fully understand the nature of interactions between nucleons. The deuteron is an ideal tool for testing the accuracy of theoretical models, and their ability to describe nuclear scattering. It is easily decomposed during the interaction and has a low binding energy (2.2 MeV). This property makes deuteron scattering highly sensitive to inelastic effects such as collective excitations of the target nucleus and channel transitions, making it an ideal probe for testing theoretical nuclear models. Although the scattering process can be complex, one of the fundamental theoretical tools for interpreting deuteron scattering on nuclei is the Optical Model Potential (OMP), which describes the complex interaction between the projectile and the target nucleus through a complex potential. In this approach, the interaction between the deuteron and the target nucleus is represented by a complex potential. This potential divides the reaction flow into a real part representing elastic scattering and an imaginary part representing all competing inelastic channels [12]. It has proven particularly effective in describing experimental data on nuclei.

The main goal of the optical model is to determine potential parameters that reproduce smooth changes in the differential scattering cross section as a function of the incident energy and the nucleon number of the target nucleus. However, the large variation in these potential parameters, such as real and imaginary depth, radius, and slope, with changes in projectile energy or nucleus type [14], represent a persistent challenge in this model and hinders its ability to predict experimental data, suggesting the presence of non-local sources in the nuclear reaction[11, 46].

One of the most important sources of non-locality in the scattering process is the coupling of inelastic excitations to the nuclear ground state during the scattering process [46]. The full effect of collective excitations is included when these channels are explicitly included using the coupled-channel model, which in turn creates a non-local dynamic polarization potential in the elastic channel as an effective component that modifies the actual potential and redistributes the flux. This, in turn, significantly improves the fit to the data and reduces the variation in the potential parameters. However, due to the large number of possible inelastic excitations, this non-locality is usually explained by the coupling of a few significant inelastic channels to the ground state [6], [17]. The dependence of optical model potential parameters on energy is reduced when channel coupling is taken into account [35].

The work of Bäumer *et al.* [2] measured angular distributions for deuteron scattering on ^{12}C, ^{24}Mg, and ^{58}Ni at 170 MeV and analyzed the data using global OM potentials with simple coupled-channels extensions. The work of ref.

Cite as: W.S. Alrayashi, East Eur. J. Phys. 3, 50 (2025), https://doi.org/10.26565/2312-4334-2025-3-05

Korff *et al.* [25] extended this approach to a broad mass range ($6 \le A \le 116$) at intermediate energies (171–183 MeV), employing CC analysis to examine the role of deformation and to adjust optical model parameters accordingly. While these studies demonstrated the relevance of coupling effects, they were limited in energy coverage, coupling schemes, and often relied on potential parameter adjustments to compensate for missing physics. The stability of parameters and the channel inclusion relationship between them have not been systematically studied quantitatively across a wide range of masses and energies. Most available global models for deuteron scattering still rely on parameters that vary with energy and the nucleus without explicitly accounting for inelastic channels.

In this work, we investigate the effectiveness of the coupled-channels analysis of deuteron elastic and inelastic scattering from a representative set of nuclei: ^{6}Li,^{12}C, ^{24}Mg, ^{58}Ni, ^{120}Sn, and ^{208}Pb. The incident deuteron energies span from 9.9 to 270 MeV also this work should give an assessment of the importance of coupling of the inelastic excitations to the ground state and hence might reduce the energy variations of the optical potential parameters with energy, thus improving our understanding of deuteron – nucleus scattering process. Using the FRESCO and SFRESCO codes [36] to solve the Coupled-Channel Schrödinger equation and hence obtain the angular distribution fits to the elastic processes in addition to simultaneous fits to the angular distributions corresponding to the most important inelastic excitations. It is a well-known fact in scattering phenomenology that more than one set of fit potential parameters lead to almost the same fit to the angular distributions data.

This article is structured as follows: Section 2 introduces the theoretical formalism of the coupled-channels method. Section 3 describes the optical model potentials and deformed nuclei. Section 4 presents the main results, including angular distribution comparisons, best-fit potential parameters, and deformation analysis. Section 5 summarizes the conclusions and outlines directions for future work.

2. COUPLED REACTION CHANNELS FORMALISM

Coupled-channel analysis is very important for describing scattering processes. When the projectile interacts with the target, they can scatter elastically, or may lead to excited states exit channels. Alternatively, rearrangement processes may occur. The coupled-channel theory is a method of accounting for inelastic channels, especially those arising from collective excitations. The formalism was first pointed out by Bohr and Mottelson [42], and then was applied by Margolis et. al. and Chase et. al. [7]. In the center-of-mass coordinate system, the total Hamiltonian $\hat{H}$ of the whole system is expressed as:

$$\hat{H} = H_p(\xi_p) + H_t(\xi_t) + \hat{T}(r) + V(r, \xi_p, \xi_t) \tag{1}$$

where r is the radial coordinate from the target to the projectile, $H_p(\xi_p)$ and $H_t(\xi_t)$ are the internal Hamiltonians for projectile and target, respectively, while the ξ_p and ξ_t are the respective internal coordinates of the projectile and target, and $V(r, \xi_p, \xi_t)$ is the interaction potential between the projectile and target, which can be written as [37]:

$$V(r, \xi_p, \xi_t) = V_{\text{diag}}(r) + V_{\text{coupl}}(r, \xi_p, \xi_t), \tag{2}$$

where $V_{\text{diag}}(r)$ is a scaler potential, and $V_{\text{coupl}}(r, \xi_p, \xi_t)$ represents the interaction that couples the initial state to the final state. Further, $\hat{T}(r)$ is the total kinetic energy, which may be written as

$$\hat{T}(r) = -\frac{\hbar^2}{2\mu}\nabla_r^2, \tag{3}$$

where $\mu = \frac{m_p m_t}{m_p + m_t}$ is the reduced mass of the projectile and target, and ∇_r^2 is the Laplacian operator. The time-independent Schrödinger equation for the whole system consisting of a projectile and a target is:

$$\hat{H}\Psi(\vec{r}, \xi_p, \xi_t) = E\Psi(\vec{r}, \xi_p, \xi_t),, \tag{4}$$

where, E is the total energy, and $\Psi(\vec{r}, \xi_p, \xi_t)$ is the wave function of the whole system. We expand $\Psi(\vec{r}, \xi_p, \xi_t)$ in terms of the eigenstates of the total angular momentum $\psi_{J_{\text{tot}}}^{\pi M_{\text{tot}}}(\vec{r}, \xi_p, \xi_t)$ as follows [37]:

$$\Psi(\vec{r}, \xi_p, \xi_t) = \sum_{\pi J_{\text{tot}} M_{\text{tot}}} A_{J_{\text{tot}} M_{\text{tot}}}\, \psi_{J_{\text{tot}}}^{\pi M_{\text{tot}}}(\vec{r}, \xi_p, \xi_t), \tag{5}$$

For each channel $[(L'S')J', I_{n'}]$, where L' is orbital angular momentum of a given partial wave, S' is projectile's spin for deuteron, $\vec{J}' = \vec{L}' + \vec{S}'$ is the total angular momentum and $I_{n'}$ is the target's spin. We couple J' and $I_{n'}$ to get the total angular momentum $\vec{J}_{tot} = \vec{J}' + \vec{I}_{n'}$ for the whole system. The factors $A_{J_{tot}M_{tot}}$ are amplitudes specifying how much of the total angular momentum state is present.The wave function $\psi_{J_{tot}}^{\pi M_{tot}}(\vec{r}, \xi_p, \xi_t)$ can be expressed as follows:

$$\psi_{J_{tot}}^{\pi M_{tot}}(\vec{r}, \xi_p, \xi_t) \quad = \quad \sum_{n'(L'S')J'I_{n'}} \psi_{n'(L'S')J'I_{n'}}^{\pi J_{tot}}(r)\, \Phi_{(L'S')J'I_{n'}}^{J_{tot}M_{tot}}(\hat{r}, \xi_p, \xi_t),$$

$$= \sum_{n'(L'S')J'I_{n'}} \frac{1}{r} R^{\pi J_{tot}}_{n'(L'S')J'I_{n'}}(r)\, \Phi^{J_{tot}M_{tot}}_{(L'S')J'I_{n'}}(\hat{r},\xi_p,\xi_t). \tag{6}$$

where $\psi^{\pi J_{tot}}_{n'(L'S')J'I_{n'}}(r) = R^{\pi J_{tot}}_{n'(L'S')J'I_{n'}}(r)/r$. The nuclear wave functions are defined as

$$\begin{aligned} \Phi^{J_{tot}M_{tot}}_{(L'S')J'I_{n'}}(\hat{r},\xi_p,\xi_t) &= [\mathcal{Y}_{(L'S')J'}(\hat{r},\xi_p)\otimes\phi_{I_{n'}}(\xi_t)]^{M_{tot}}_{J_{tot}} \\ &= \sum_{M_{J'}m_{I_{n'}}} < J'I_{n'}M_{J'}m_{I_{n'}} \mid J_{tot}M_{tot} > \mathcal{Y}_{(L'S')J'M_{J'}}(\hat{r},\xi_p) \\ &\times\ \phi^{m_{I_{n'}}}_{I_{n'}}(\xi_t), \end{aligned} \tag{7}$$

and the spin-angle functions are defined as

$$\begin{aligned} \mathcal{Y}_{(L'S')J'M_{J'}}(\hat{r},\xi_p) &= [Y^{M_{L'}}_{L'}(\hat{r})\otimes\chi^{m_{s'}}_{S'}(\xi_p)]^{M_{J'}}_{J'} \\ &= \sum_{M_{L'}m_{s'}} < L'S'M_{L'}m_{s'} \mid J'M_{J'} > i^{L'}Y^{M_{L'}}_{L'}(\hat{r})\,\chi^{m_{s'}}_{S'}(\xi_p), \end{aligned} \tag{8}$$

where, $R^{\pi J_{tot}}_{n'(L'S')I_{n'}}(r)$ are the radial wave functions in the excited state n', and n' corresponds to the n'th state of the target, while $Y^{M_{L'}}_{L'}(\hat{r})$ are the spherical harmonics. The phase factor $i^{L'}$ comes from the spherical Bessel expansion of the incident plane wave. The symbol $\otimes$ denotes vector addition, and $< L'S'M_{L'}m_{s'} \mid J'M_{J'} >$ are Clebsch-Gordon coefficients for coupling $L'M_{L'}$ and $S'm_{s'}$ to intermediate angular momenta $J'M_{J'}$. In addition, $< J'I_{n'}M_{J'}m_{I_{n'}} \mid J_{tot}M_{tot} >$ are the Clebsch-Gordon coefficients for coupling $J'M_{J'}$ and $I_{n'}m_{I_{n'}}$ to a total of angular momentum $J_{tot}M_{tot}$ for the whole system. Further, $\phi^{m_{I_{n'}}}_{I_{n'}}(\xi_t)$ and $\chi^{m_{s'}}_{S'}(\xi_p)$ are the wave functions for target and projectile, respectively, and π is the parity operator of the whole system which can be expressed as:

$$\pi = (-1)^{L'}\pi_{s'}\pi_{I_{n'}}. \tag{9}$$

The nuclear wave function can be written as

$$\begin{aligned} \Phi^{J_{tot}M_{tot}}_{(L'S')J'I_{n'}}(\hat{r},\xi_p,\xi_t) &= [Y^{M_{L'}}_{L'}(\hat{r})\otimes\chi^{m_{s'}}_{S'}(\xi_p)\otimes\phi^{m_{I_{n'}}}_{I_{n'}}(\xi_t)]^{M_{tot}}_{J_{tot}} \\ &= \sum_{M_{J'}m_{I_{n'}}}\sum_{M_{L'}m_{s'}} i^{L'}Y^{M_{L'}}_{L'}(\hat{r})\,\chi^{m_{s'}}_{S'}(\xi_p)\,\phi^{m_{I_{n'}}}_{I_{n'}}(\xi_t) \\ &\times\ < L'S'M_{L'}m_{s'} \mid J'M_{J'} >< J'I_{n'}M_{J'}m_{I_{n'}} \mid J_{tot}M_{tot} >,, \end{aligned} \tag{10}$$

Now, by substituting Eqs. (5), (6), and (10) into Eq. (4) and noting that :

$$\begin{aligned} &H_p(\xi_p)\,\chi_p(\xi_p) = E_p\,\chi_p(\xi_p), \\ &H_t(\xi_t)\,\phi_t(\xi_t) = E_t\,\phi_t(\xi_t). \end{aligned} \tag{11}$$

Here, E_p and E_t are the eigenenergies for the projectile and the target, respectively. one obtains

$$\sum_{n'J'I_{n'}S'L'}\left[\hat{T}_{n'L'} + V(r,\xi_p,\xi_t) - E_{n'}\right]R^{\pi J_{tot}}_{n'L'S'J'I_{n'}}(r)\,\Phi^{J_{tot}M_{tot}}_{(L'S')J'I_{n'}}(\hat{r},\xi_p,\xi_t) = 0,$$

where

$$\hat{T}_{n'L'} = \frac{\hbar^2}{2\mu_{n'}}\left[-\frac{d^2}{dr^2} + \frac{L'(L'+1)}{r^2}\right], \tag{12}$$

where $E_{n'} = E - E_p - E_t$ is the external energy for a given excited state. Multiplying Eq. (12) by $[\Phi^{J_{tot}M_{tot}}_{(L'S')J'I_{n'}}(\hat{r},\xi_p,\xi_t)]^*$ from the left, and integrating over the internal coordinates except the radial variable r, leads to the following partial wave coupled differential equations: Finally, the coupled partial-wave equations take the form

$$\begin{aligned} &\left[E_{n_i} - \hat{T}_{n_iL} - V_{(LS)JI_{n_i};(LS)JI_{n_i}}(r)\right]R^{\pi J_{tot}}_{n_iLSJI_{n_i}}(r) \\ &= \sum_{n'L'S'J'I_{n'}} V_{(LS)JI_{n_i};(L'S')J'I_{n'}}(r)R^{\pi J_{tot}}_{n'L'S'J'I_{n'}}(r). \end{aligned} \tag{13}$$

This equation represents a set of n' coupled differential equations for the radial wave functions $R^{\pi J_{tot}}_{n_i LSJI_{n_i}}(r)$ and $R^{\pi J_{tot}}_{n'L'S'J'I_{n'}}(r)$. Furthermore, $V_{(LS)JI_{n_i};(LS)JI_{n_i}}(r)$ is the diagonal optical potential, including both coulomb and nuclear parts, and $V_{(LS)JI_{n_i};(L'S')J'I_{n'}}(r)$ represent the coupling interaction of the initial $(LS)JI_{n_i}$ state to the final $(L'S')J'I_{n'}$ state. Nuclear structure deformations affect the matrix elements on the right-hand side of Eq. (13). For a non-deformed target nucleus, the coupling potential vanishes, and the set of coupled differential equations reduces to that of the Schrödinger equation for a single channel. Deformed nuclei can be described using either the vibrational or rotational models. In this work, we use the optical model and coupled-channel analysis to couple the ground state to collective excited states of the target nucleus. This coupling introduces off-diagonal couplings in the interaction potential matrix, allowing the incident deuteron to induce transitions from the ground state to inelastic states. These coupling potentials, typically derived from nuclear deformation (e.g., using a deformation parameter β_λ), significantly affect observables such as scattering cross sections and resonance structures. As a result, including channel coupling provides a more accurate description of the reaction dynamics.

3. THE OPTICAL POTENTIAL PARAMETERS

The optical model describes the complicated interaction between the projectile and target in terms of a complex potential. This potential divides the reaction flux into a real part, which corresponds to elastic scattering, and an imaginary part, which corresponds to all competing inelastic channels [11]. The aim of the optical model is to find a potential that describes smooth variations of the scattering cross section as a function of incident energy E and target nucleon number A. The general situation of scattering may be quite complicated. However, great simplification may be obtained if one is only interested in the averaged properties, away from resonances and states strongly excited by direct reactions. For deuteron-nucleus scattering, the phenomenological optical potential, $V(r, E)$, can be expressed as [37]

$$\begin{aligned} V(r,E) &= -\Big(V(E) + iW_v(E)\Big) f(r,R_v,a_v) + i4a_sW_s(E)\frac{d}{dr}f(r,R_s,a_s) \\ &+ \Big(V_{so} + iW_{so}\Big)\Big(\frac{\hbar}{m_\pi c}\Big)^2\frac{1}{r}\frac{d}{dr}f(r,R_{so},a_{so})\vec{L}\cdot\vec{\sigma} + V_{\mathrm{Coul}}(r), \end{aligned} \tag{14}$$

where $V(E)$, V_{so} are the real components of the volume-central and spin-orbit potentials, respectively. In addition, $W_v(E)$, $W_s(E)$, and W_{so} are the imaginary components of volume, surface, and spin orbit potentials, respectively, and $V_{\mathrm{Coul}}(r)$ is the coulomb potential. E is the energy of the incident particle in the laboratory frame. As for the radial dependence of the potential, the well-known realistic Woods-Saxon form factor is used [24]:

$$\begin{aligned} V_v(r) &= V(E)f(r,R_v,a), \\ W_v(r) &= W_v(E)f(r,R_v,a), \\ W_s(r) &= -4a_sW_s(E)\frac{d}{dr}f(r,R_s,a), \\ V_{so}(r) &= V_{so}\Big(\frac{\hbar}{m_\pi c}\Big)^2\frac{1}{r}\frac{d}{dr}f(r,R_{so},a_{so}), \\ W_{so}(r) &= W_{so}\Big(\frac{\hbar}{m_\pi c}\Big)^2\frac{1}{r}\frac{d}{dr}f(r,R_{so},a_{so}), \end{aligned} \tag{15}$$

where m_π is the pion mass. The form factor $f(r, R_i, a_i)$ is the Saxon-Woods shape[41],

$$f(r,R_i,a_i) = \frac{1}{1+\exp[(r-R_i)/a_i]}\,, \qquad i = v, s, so, c \tag{16}$$

where, $R_i = r_iA^{\frac{1}{3}}$ is a potential radius, A the mass number of the target, and a_i the diffuseness parameters. For charged projectiles, the Coulomb term $V_{\mathrm{Coul}}(r)$ is usually obtained by approximating the target nucleus as a uniformly charged sphere,

$$V_{\mathrm{Coul}}(r) = Z_pZ_te^2\int\frac{\rho(r_t)}{|\,\vec{r}-\vec{r}_t\,|}\,d\vec{r}_t, \tag{17}$$

where $\vec{r}$ is the position of the projectile and $\vec{r}_t$ is that of target nucleus. The quantities Z_p and Z_t are the atomic numbers of the projectile and target, respectively. The term $\rho(r_t)$ gives the charge distribution in the target.

Deformed nuclei, whose surfaces vibrate about an equilibrium shape, are treated using the vibrational model. Here, the dynamic nuclear radius R_i is taken to be a function of the polar angles θ and ϕ according to:

$$R_i(\theta,\phi) = r_iA^{\frac{1}{3}}\Bigg[1 + \sum_{\lambda\geq 1}^{\infty}\sum_{\mu=-\lambda}^{\mu=\lambda}\alpha_{\lambda\mu}Y_{\lambda\mu}(\theta,\phi)\Bigg], \tag{18}$$

where $R_i(\theta,\phi)$ is the distance from the center of the nucleus to a point at its surface subtending polar and azimuthal angles (θ,ϕ). The spherical tensors $\alpha_{\lambda\mu}$ are the spherical harmonics $(Y_{\lambda\mu}(\theta,\phi))$ coefficients. However, some nuclei have permanent deformations about a symmetry axis and are treated using the rotational model. In this case the nuclear radius is expressed in the form:

$$R_i(\theta') = r_i A^{\frac{1}{3}}\left[1 + \sum_{\lambda}\beta_\lambda Y_{\lambda 0}(\theta')\right], \tag{19}$$

where, θ' is the polar angle in the body - fixed frame and β_λ is the deformation parameter. When the vibrational or rotational models are used, one has to determine which parts of the potential are to be deformed. Since the nuclear force is a short range force the nuclear potential follows the shape of the nucleus. Therefore, it is a common practice to deform the volume term of the potential. Deforming the imaginary surface part, however, is a matter of dispute. This issue has been discussed and arguments were presented in support and also against deforming the imaginary surface part [5]. However, in a later work [16], the authors stated that "to describe the inelastic scattering best, it is found necessary to deform the imaginary (as well as the real) part of the central potential." Furthermore, in Ref. [2] and [25] the authors used an optical model with channel coupling to analyze deuteron induced reactions. All parts of the nuclear potential were deformed except the spin-orbit term. In Ref. [35] we examined the effect of channel coupling on the variation of the potential parameters corresponding to nucleon scattering off light and heavy nuclei. We obtained excellent angular distribution fits for the elastic and inelastic channels by deforming both the real volume and imaginary surface terms. Therefore, in this work, we shall deform the surface imaginary term in addition to the real volume term. We did not deform the spin - orbit term as the effects of its deformation on the calculated differential cross sections were found to be insignificant [21].

4. RESULTS AND DISCUSSION

This section presents a detailed analysis of deuteron elastic and inelastic scattering from ^{6}Li, ^{12}C, ^{24}Mg, ^{58}Ni, ^{120}Sn, and ^{208}Pb nuclei over an incident energy range spanning from 9.9 to 270 MeV. The theoretical framework employed is the coupled-channels (CC) method, implemented using the FRESCO and SFRESCO codes developed by Thompson [36]. These codes allow for systematic inclusion of couplings between the ground and excited states of the target nuclei, facilitating a unified treatment of elastic and inelastic scattering processes within a consistent reaction model. The main goal of this study is to investigate the effect of ground state coupling to inelastic reaction channels on the energy variations of the optical potential parameters. In doing so, we have used the rotational model to analyze the deuteron elastic and inelastic excitation differential cross sections. The optical potential parameters were obtained by fitting the coupled-channels differential cross sections $d\sigma_{n_i n'}(\theta)/d\Omega$, the experimental data for the elastic and inelastic scattering cross sections for light and heavy nuclei were taken from the Experimental Nuclear Reaction Data (EXFOR) and the Computer Index of Nuclear Reaction Data (CINDA) are displayed in Table 1. The coupled channel analysis shows that nuclei become deformed when the potential couples the ground state to the inelastic excited states. In deformed nuclei, the non-diagonal potential couples the ground state to the inelastic excited states. So, the deformation lengths $\delta_\lambda = \beta_\lambda R$ were extracted by fitting the experimental data of the coupled channels differential cross sections for collective excitations. The multipolarity λ of the reaction can be represented as follows: For $\lambda = 2$, we have quadrupole deformations β_2 [30] and [32]. For $\lambda = 3$ we have octupole deformations β_3 [40]. For $\lambda = 5$ we have quintupole deformations β_5. In order to compare the optical potential parameter calculations with the experimental results, we used the automatic search routine of SFRESCO. This program minimizes the chi-squared value χ^2, which is defined as:

$$\chi^2 = \frac{1}{N}\sum_{i=1}^{N}\left(\frac{\left(\frac{d\sigma(\theta_i)}{d\Omega}\right)_{\text{theo}} - \left(\frac{d\sigma(\theta_i)}{d\Omega}\right)_{\text{exp}}}{\Delta\left(\frac{d\sigma(\theta_i)}{d\Omega}\right)}\right)^2, \tag{20}$$

where N is the number of experimental points, $(\frac{d\sigma(\theta_i)}{d\Omega})_{theo}$ and $(\frac{d\sigma(\theta_i)}{d\Omega})_{exp}$ are the theoretical and experimental differential cross sections at the angle θ_i, and $\Delta(\frac{d\sigma(\theta_i)}{d\Omega})$ is the corresponding experimental error. We now proceed to discuss the results obtained by fitting the experimental elastic and inelastic differential cross sections. For all the nuclei studied in this work, we have considered incident deuteron energies where EXFOR provides the experimental data for the elastic scattering and inelastic excitations. This enables us to study the effect of ground-state coupling to open reaction channels on the energy variation of the optical potential parameters. It is well known that more than one set of optical potential parameters can fit a given experimental dataset.

Table 1. Experimental data for deuteron elastic and inelastic scattering for the nuclei and energies considered in this work were collected from the EXFOR and CINDA databases.

Nucleus	E **(MeV)**	**Ref.**
^{6}Li	14.8, 25.0	[10]
	171	[2]
^{12}C	11.8	[51]
	13.7, 15.3, 25.9	[52]
	60.6	[54]
	77.3, 90	[55]
	170	[2]
	200	[56]
	270	[57]
^{24}Mg	9.97, 10.9, 12.1, 15.3, 21	[52]
	60.6	[54]
	77.3, 90	[55]
	170	[2]
^{58}Ni	12, 12.8	[58]
	27.5	[59]
	79.9	[60]
	170	[2]
^{120}Sn	13.6	[10]
	28.6	[52]
	80, 82	[49]
^{208}Pb	86	[57]

Coupling of the Elastic Channel to a Single Excited State in ^{6}Li and ^{12}C

A detailed coupled-channels analysis was performed for deuteron elastic and inelastic scattering from the light ^{6}Li, and ^{12}C nuclei. Light nuclei differ from heavy ones in that their matter distributions are less uniform. They have diffused edges that results in surface effects playing an important role in the scattering processe. In order to test the effect of channel coupling on the energy variation of the optical potential parameters, we begin by coupling the elastic channel to the first excited state. The diagonal and coupling optical potentials given in Eq. (2) were used to fit the elastic and inelastic angular distributions simultaneously. The analysis of the ^{6}Li data was restricted to coupling the 1^{+} ground state to the first 3^{+} excited state, whose excitation energy is $E_x = 2.186$ MeV. As shown in Fig. 1, the fits for the angular distributions show good agreement with the experimental data for the elastic (1^{+}) and the first (3^{+}) excited channels for incident energies of 14.8, 25, and 171 MeV. The corresponding optical potential best fit parameters as a function of incident energy when the elastic and first excited channels are coupled together, are displayed in Table 2. For ^{12}C ,a well-studied nucleus over the energy range 11.8 to 270 MeV, variations in the angular distributions are strongly influenced by coupling to the ground state via collective transitions. We coupled the 0^{+} elastic channel to the first 2^{+} excited state ($E_x = 4.438$ MeV). The corresponding fits for the elastic 0^{+} and inelastic 2^{+} differential cross sections show very good agreement with the experimental data as seen in Fig 2. The optical model parameters corresponding to these fits are listed in Tables 3 and 4. In our fitting procedure, we also searched for the best value of the quadrupole deformation parameter β_2 at each incident energy. Assuming all the obtained values to have the same weight, our average value for the quadrupole deformation is $\beta_2 = 1.39$ for ^{6}Li, which is in good agreement with the value β_2=0.89 obtained in Ref. [25]. In addition, our mean value for the quadrupole deformation is β_2=0.73 for ^{12}C, which is in good agreement with the value β_2=0.60 obtained in Ref. [9].

Table 2. The optical potential best fit parameters for ^{6}Li$(d,d)^6$Li* scattering cross sections for the elastic (1^+) and 3^+ excited state. The Coulomb radius was fixed at r_c = 1.2 fm.

Parameters	14.8 MeV	25.0 MeV	171.0 MeV
V (MeV)	89.990	70.090	28.600
r (fm)	1.160	0.910	1.400
a (fm)	0.900	0.220	0.900
W_s (MeV)	5.280	2.160	7.690
r_s (fm)	1.400	1.540	1.080
a_s (fm)	0.900	0.890	0.830
V_{so}(MeV)	2.000	4.790	2.288
r_so (fm)	0.800	1.040	1.420
a_so (fm)	0.900	0.300	0.900
β_2 (fm)	1.29	2.07	0.786
χ^2	99.200	1.075	189.600

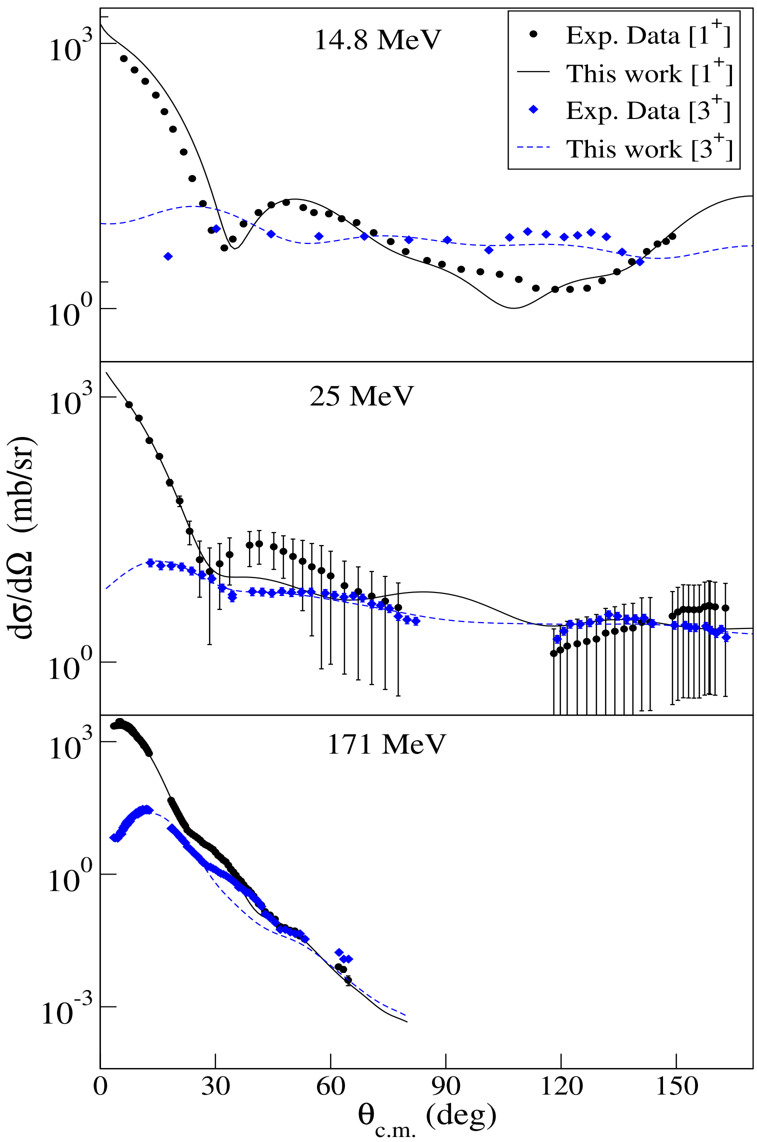

Figure 1. (Color online) Elastic and inelastic best angular distribution fits for deuteron scattering from ^{6}Li.

Table 3. The optical potential best fit parameters for $^{12}C(d,d)^{12}C^*$ scattering cross sections for the elastic (0^+) and (2^+) excited state. The Coulomb radius was fixed at r_c = 1.2 fm.

Parameters	11.8 MeV	13.7 MeV	15.3 MeV	25.9 MeV	60.6 MeV
V (MeV)	63.00	62.00	61.9999	54.4645	52.00
r (fm)	0.9956	1.0000	1.0154	1.0562	0.8306
a (fm)	0.8500	0.7958	0.8100	0.7499	0.4137
W_s (MeV)	13.00	12.7351	11.1303	13.00	10.00
r_s (fm)	1.2033	1.2233	1.2343	1.0718	1.0000
a_s (fm)	0.3522	0.3672	0.4029	0.4301	0.5567
V_{so} (MeV)	4.0385	5.1000	3.8314	4.0000	4.5000
r_{so} (fm)	0.9000	0.8152	0.7646	1.0524	0.8855
a_{so} (fm)	0.4512	0.3000	0.3010	0.7000	0.7500
β_2	0.659	0.656	0.606	0.730	0.789
χ^2	10.150	10.049	69.195	69.195	6.194

Table 4. The optical potential best fit parameters for $^{12}C(d,d)^{12}C^*$ scattering cross sections for the elastic (0^+) and (2^+) excited state. The Coulomb radius was fixed at r_c = 1.2 fm.

Parameters	77.3 MeV	90.0 MeV	170.0 MeV	200.0 MeV	270.0 MeV
V (MeV)	45.09	40.00	40.00	37.84	31.27
r (fm)	0.800	0.936	0.940	0.900	0.970
a (fm)	0.495	0.850	0.410	0.390	0.440
W_s(MeV)	10.00	18.54	13.00	17.00	16.99
r_s (fm)	0.930	0.904	1.070	1.170	1.109
a_s (fm)	0.714	0.654	0.780	0.710	0.800
V_{so}(MeV)	6.10	4.50	4.03	4.00	4.00
r_{so} (fm)	0.800	0.800	0.840	0.900	0.800
a_{so} (fm)	0.750	0.400	0.800	0.600	0.800
β_2 (fm)	0.966	0.699	0.743	0.776	0.720
χ^2	30.90	49.82	73.45	8.860	6.300

When the elastic channel and the first excited states are coupled together for ^{6}Li, and ^{12}C, we find that the variations of all OMP parameters are reduced. It is clear from Tables. 2 –4 that the value of V decreased with increasing energy, but its variation is reduced as shown in Fig. (3). In addition, the variations of V for the ^{12}C case are similar to the variations in the ^{6}Li case as can be seen in Figures (3). The variation in the surface absorption depth W_s is smaller and remains highly stable as a function of incident energy for ^{6}Li and ^{12}C. Channel coupling has also resulted in the real part of the spin-orbit potential V_{so} being almost constant over the entire energy range around 4.0 MeV for these nuclei. In previous work, Ref. [1]fixed the value of V_{so} at 3.557 MeV, while V_{so} was taken as 3.703 MeV in Ref. [20], 6.0 MeV in Ref. [3].,and 5.5 MeV in Ref. [10]. The variations in the geometric parameters (r, r_s, r_{so}) and (a, a_s, a_{so}) are also highly stable, as shown in Fig. (3). The mean $\bar{\chi}^2$ value for light nuclei is approximately 65 when the elastic channel is coupled with the first excited state.

In what follows, we study the effect of coupled-channel analysis on the energy dependence of the optical potential parameters for heavy nuclei

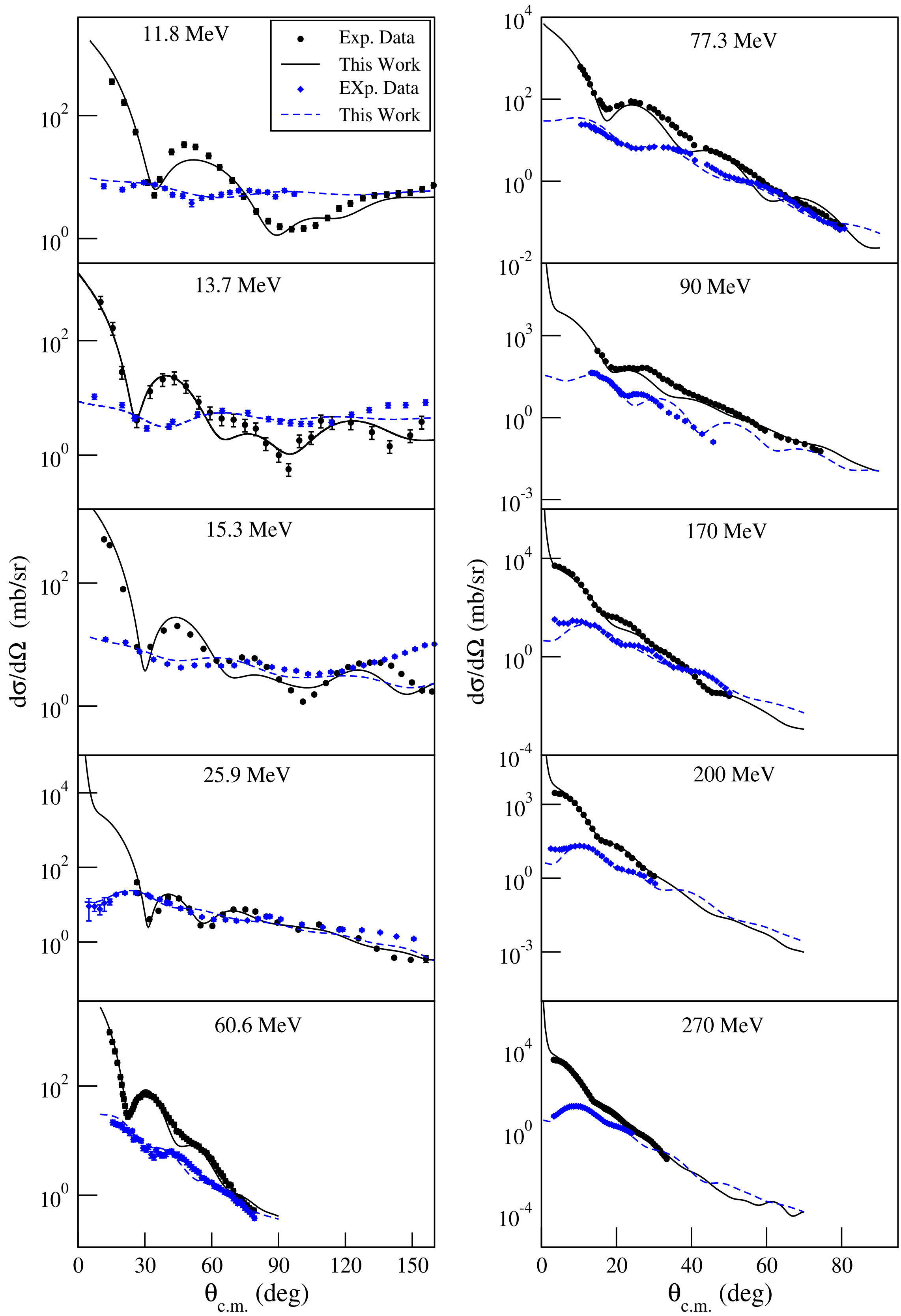

Figure 2. (Color online) Elastic and inelastic best angular distribution fits for deuteron scattering from ^{12}C.

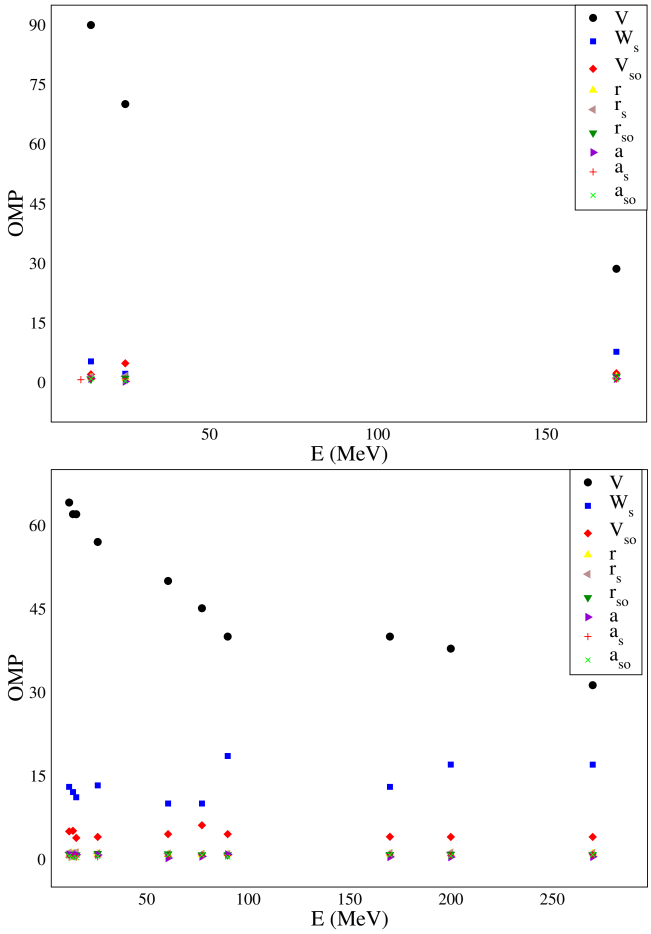

Figure 3. (Color online) The variations of the optical potential depths as a function of incident energy for ^{6}Li (top), ^{12}C (bottom).

Coupling the Ground State of ^{24}Mg, ^{58}Ni, ^{120}Sn, and ^{208}Pb to Collective Excited States

In this section, we investigate the effect of coupled-channels analysis on the optical model parameters for intermediate and heavy nuclei. Heavy nuclei have almost constant matter densities up to large distances away from the nuclear center. Therefore, surface effect, which result in larger energy dependence of the optical potential parameters, are expected to play a reduced role compared to the case of light nuclei. All this is expected to result in more stable optical potential parameters as a function of energy. We present a detailed coupled-channels analysis of deuteron elastic and inelastic scattering on the ^{24}Mg, ^{58}Ni, ^{120}Sn, and ^{208}Pb nuclei over an energy range of 9.9 to 170 MeV. Here, we coupled the 0^+ elastic channel and the first 2^+ excited state corresponding to deuteron scattering from ^{24}Mg, ^{58}Ni, ^{120}Sn, where the respective excitation energies are 1.368 MeV, 1.454 MeV, and 1.171 MeV, respectively. The obtained results for the elastic 0^+ and inelastic 2^+ differential cross sections show excellent agreement with the experimental data as displayed in Figs. (4) to (6). Our fitting procedure also resulted in best-fit for the quadrupole deformation $\beta_2 = 0.64$, $\beta_2 = 0.244$, and $\beta_2 = 0.097$ for coupling the ground state of ^{24}Mg, ^{58}Ni, and ^{120}Sn to the 2^+ excited state, respectively, which are in good agreement with previous work, where the corresponding values of $\beta_2 = 0.605$, $\beta_2 = 0.182$ and $\beta_2 = 0.107$ obtained in Refs. [31].

In the case of ^{208}Pb scattering, we coupled the 0^+ ground state to the 3^- (2.6146 MeV) inelastic excited state at energy 86 MeV for which experimental data are available. The corresponding excellent angular distribution fits are shown in Figure (7). In the coupling between the 0^+ (elastic channel) and first 3^- excited state for the target nucleus ^{208}Pb, an octupole deformation parameter $\beta_3 = 0.11$ was obtained, which is in a good agreement with previous work is $\beta_3 = 0.11$ of [15]. In addition, we shall consider the effect of coupling the ground state to two inelastic channels on the optical potential parameters for ^{208}Pb, when the 0^+ ground state is coupled to the 3^- (2.6146 MeV) and 5^- (3.197 MeV) excited states. In this case, the calculated elastic and inelastic differential cross sections show excellent agreement with experimental data at an incident energies of 86 Mev as shown in Figure (7), and our fitted values are $\beta_3 = 0.11$ for an octupole deformation and $\beta_5 = 0.0563$ for the quintupole deformation. Furthermore, Tables (5) to (9) show the optical potential best fit parameters as a function of incident deuteron energy for the ^{24}Mg to ^{208}Pb target nuclei when the elastic channel and excited states are coupled together. Similar to the case of light nuclei, when the ground state is coupled to the first excited state the energy variations of optical potential parameters are reduced.

Table 5. The optical potential best fit parameters for $^{24}Mg(d,d)^{24}Mg^*$ scattering cross sections for the elastic (0^+) and (2^+) excited state. The Coulomb radius was fixed at $r_c = 1.2$ fm.

Parameters	9.97 MeV	10.87 MeV	12.10 MeV	15.30 MeV	21.00 MeV
V (MeV)	73.000	71.545	65.753	66.000	54.216
r (fm)	1.0000	1.0000	1.0281	1.0255	1.0000
a (fm)	0.7712	0.7034	0.5959	0.7163	0.6584
W_s (MeV)	16.000	16.000	16.000	16.000	13.000
r_s (fm)	1.2023	1.1508	1.0765	1.1163	0.9354
a_s (fm)	0.4403	0.4334	0.4721	0.4511	0.6261
V_{so} (MeV)	5.7434	5.0000	5.0000	7.2000	5.0000
r_{so} (fm)	0.9095	0.9000	0.9000	0.9000	0.9870
a_{so} (fm)	0.3000	0.3629	0.3041	0.3624	0.7500
β_2	0.520	0.520	0.506	0.507	0.520
χ^2	4.958	10.127	20.257	150	7.128

Table 6. The optical potential best fit parameters for $^{24}Mg(d,d)^{24}Mg^*$ scattering cross sections for the elastic (0^+) and (2^+) excited state. The Coulomb radius was fixed at $r_c = 1.2$ fm.

Parameters	60.6 MeV	77.3 MeV	90.0 MeV	170.0 MeV
V (MeV)	61.999	55.000	53.120	32.384
r (fm)	0.874	0.900	1.000	0.912
a (fm)	0.778	0.494	0.800	0.576
W_s(MeV)	14.632	16.000	15.000	13.836
r_s (fm)	0.928	0.935	0.900	1.027
a_s (fm)	0.614	0.669	0.800	0.763
V_{so}(MeV)	4.000	4.000	4.000	3.092
r_{so} (fm)	0.800	0.800	0.800	0.879
a_{so} (fm)	0.500	0.400	0.800	0.600
β_2 (fm)	0.764	0.805	0.693	0.950
χ^2	12.478	26.833	19.562	128.475

Table 7. The optical potential best fit parameters for $^{58}Ni(d,d)^{58}Ni^*$ scattering cross sections for the elastic (0^+) and (2^+) excited state. The Coulomb radius was fixed at $r_c = 1.2$ fm.

Parameters	11.8 MeV	13.6 MeV	27.5 MeV	80.0 MeV	170.0 MeV
V(MeV)	83.000	74.591	78.000	59.999	47.783
r(fm)	1.100	1.196	0.950	1.017	0.916
a(fm)	0.747	0.748	0.780	0.585	0.549
W_s(MeV)	15.000	14.990	15.430	12.000	15.000
r_s(fm)	1.220	1.369	1.060	0.913	1.010
a_s (fm)	0.690	0.666	0.630	0.727	0.749
V_{so}(MeV)	6.000	5.555	4.000	4.913	3.000
r_{so} (fm)	1.100	1.265	1.130	0.906	0.921
a_{so} (fm)	0.700	0.300	0.300	0.205	0.700
β_2 (fm)	0.282	0.222	0.293	0.166	0.257
χ^2	8.448	7.455	4.990	3.865	42.151

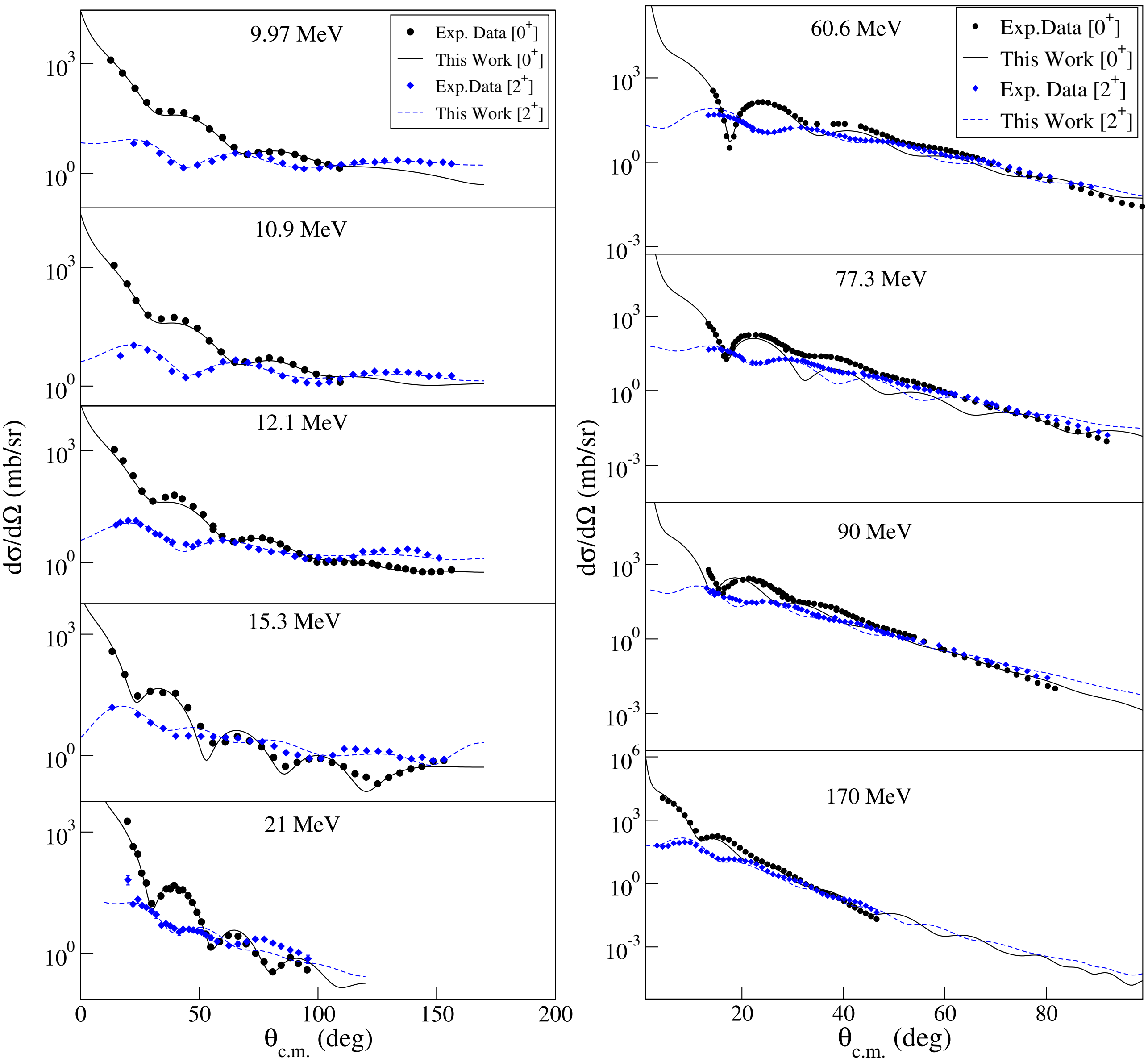

Figure 4. (Color online) Comparison between experimental angular distributions and results of OMP calculations with coupled channles computations for deuteron elastic and inelastic scattering from ^{24}Mg.

Table 8. The optical potential best fit parameters for ^{120}Sn$(d,d)^{120}$Sn* scattering cross sections for the elastic (0^+) and (2^+) excited state. The Coulomb radius was fixed at $r_c = 1.2$ fm.

Parameters	13.6 MeV	28.6 MeV	82.0 MeV
V(MeV)	68.09	69.11	60.00
r(fm)	1.160	1.140	1.460
a(fm)	0.540	0.220	0.440
W_s(MeV)	13.00	7.64	15.21
r_s (fm)	0.900	1.230	1.200
a_s (fm)	0.860	0.810	0.630
V_{so}(MeV)	4.37	6.00	4.27
r_{so} (fm)	1.210	1.240	1.260
a_{so} (fm)	0.300	0.300	0.400
β_2 (fm)	0.161	0.089	0.042
χ^2	3.530	16.90	22.40

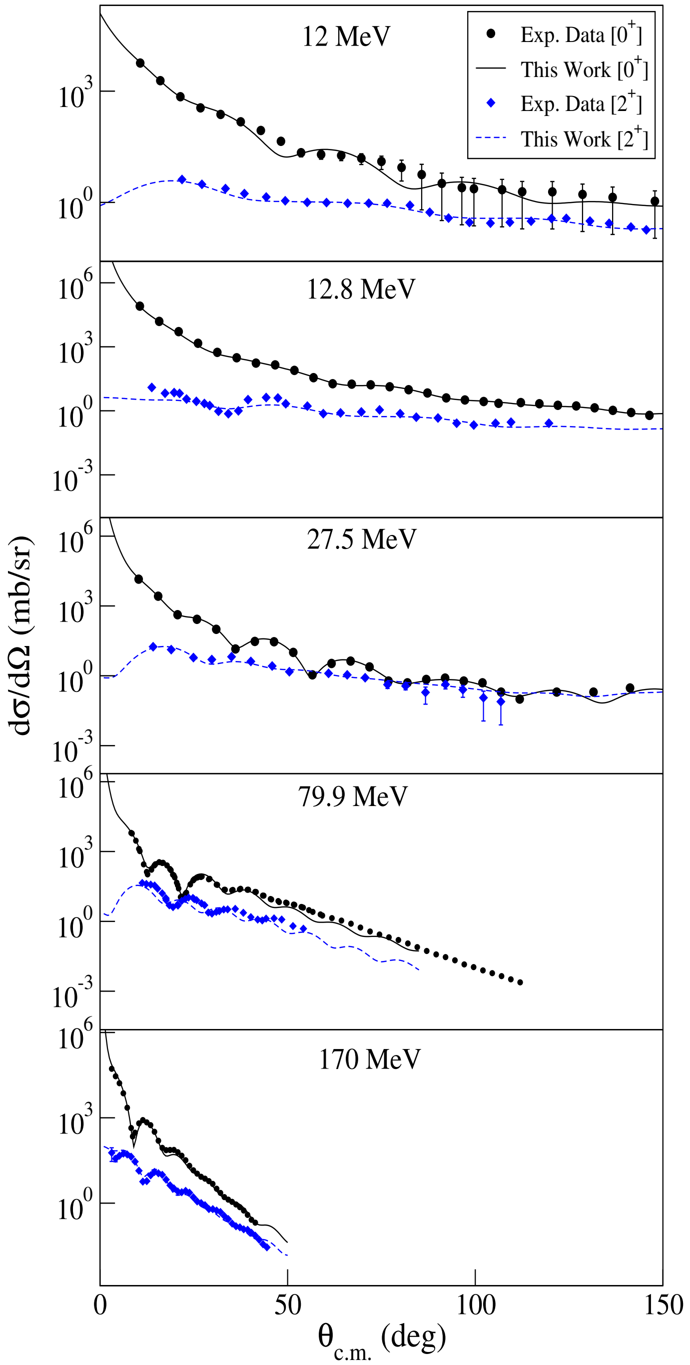

Figure 5. (Color online) Elastic and inelastic best angular distribution fits for deuteron scattering from ^{58}Ni.

Table 10. Theoretical predictions of deformation parameters compared to previous works. Where the values previous works are given in [a [9], b [38], c [31], d [19], e [15], f [39]].

	Target nucleus					
Def.Parameter	^{6}Li	^{12}C	^{24}Mg	^{58}Ni	^{120}Sn	^{208}Pb
β_2		0.582^a	0.600^c	0.182^d	0.107^d	
	1.39	0.73	0.64	0.24	0.097	
β_3						0.110^e
						0.11
β_5						0.056

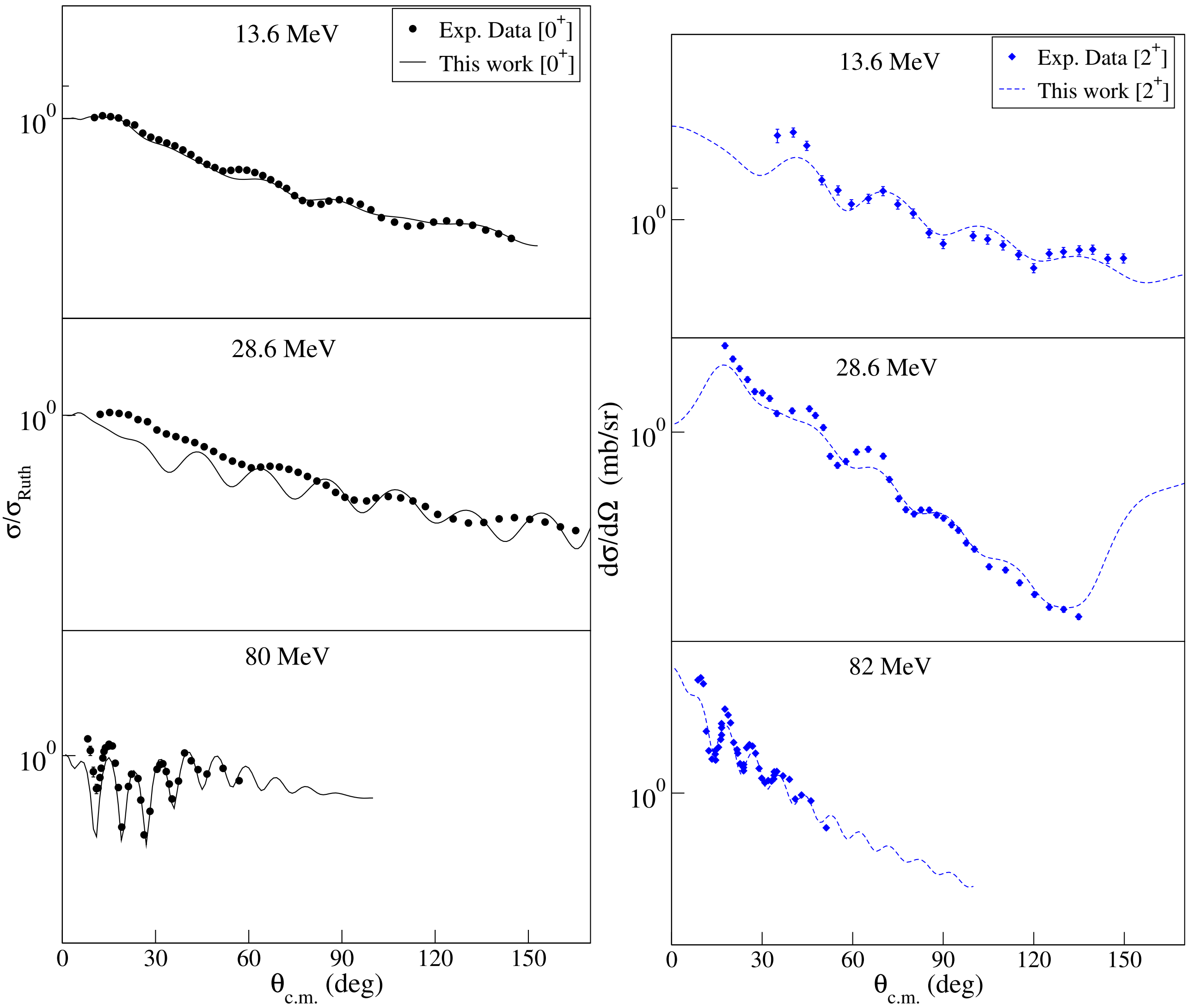

Figure 6. (Color online) Comparison between experimental angular distributions and results of OMP calculations with coupled channles computations for deuteron elastic and inelastic scattering from ^{120}Sn.

Table 9. The optical potential best fit parameters for ^{208}Pb$(d,d)^{208}$Pb* scattering cross sections for the elastic (0^+) and $(3^-,5^-)$ excited state. The Coulomb radius was fixed at $r_c = 1.2$ fm.

Parameters	Coupling $(0^+, 3^-, 5^-)$ 86.0 MeV	Coupling $(0^+, 3^-)$ 86.0 MeV
V(MeV)	37.34	35.86
r(fm)	1.09	1.12
a(fm)	0.80	0.80
W_s(MeV)	15.99	16.0
r_s (fm)	0.99	1.05
a_s (fm)	0.89	0.77
V_{so}(MeV)	4.0	4.0
r_{so}(fm)	0.98	1.08
a_{so}(fm)	0.64	0.30
β_3(fm)	0.103	0.099
β_5(fm)	0.018	-
χ^2	6.6	4.08

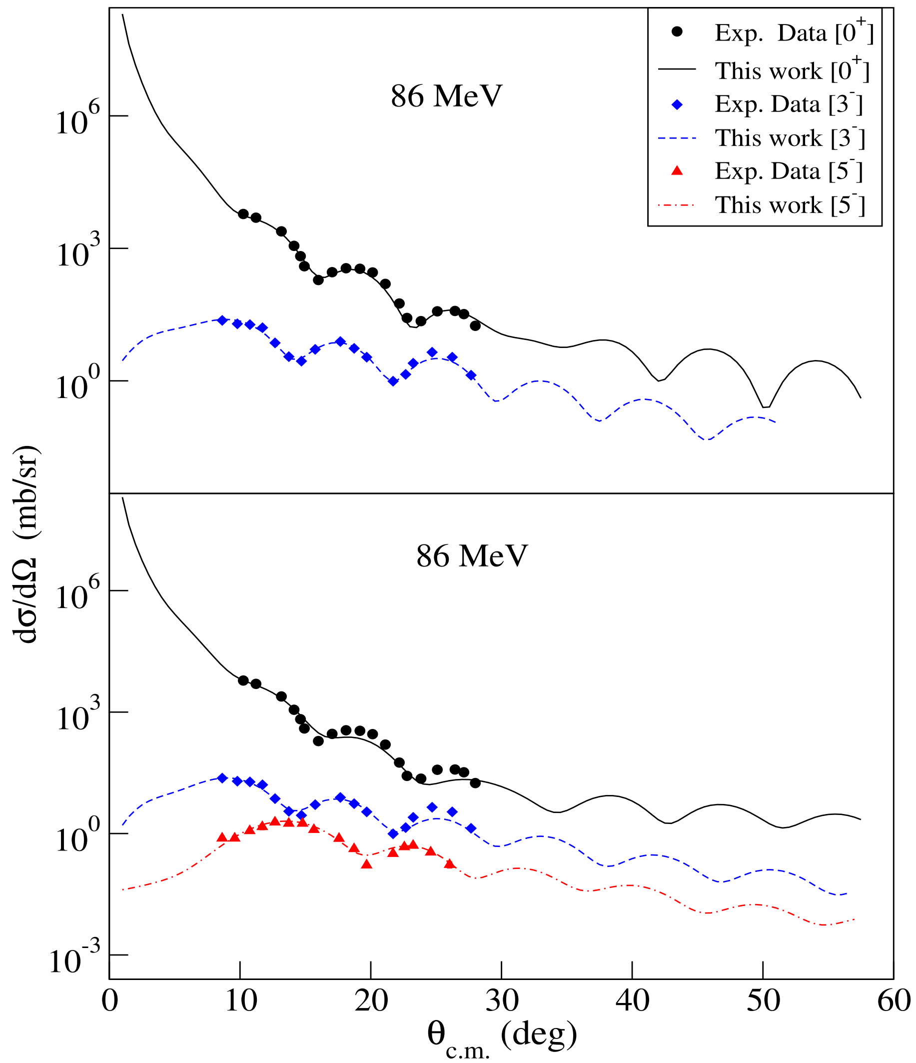

Figure 7. (Color online) Elastic and inelastic best angular distribution fits for deuteron scattering from ^{208}Pb.

Clearly, for all the considered nuclei, we found that the variations in the optical potential parameters with incident energy are reduced. Coupling the 0^+ elastic channel with the first excited state in ^{24}Mg ^{58}Ni, and ^{120}Sn the variations in the real part of the central potential V are smaller, and its value decreased with increased incident energy, as expected. In addition, it can be noted that the behavior of the surface absorption term W_s remains more stable as a function of incident energy for the ^{24}Mg, ^{58}Ni, ^{120}Sn nuclei, as shown in Figs. 8. The real part of the spin-orbit depth (V_{so}) remains highly stable when channel coupling is taken into account. The results of this work yield $V_{so} \approx 4.0$ MeV, as shown in Figs. 8 for heavy nuclei.

Previous works have reported $V_{so} \approx 3.557$ MeV [1], 3.703 MeV [20], and 6.0 MeV [3], and 5.5 MeV in Ref.[10]. The geometric parameters (r, r_s, r_{so}) and (a, a_s, a_{so}) are more stable. For heavy nuclei, our mean value of $\bar{\chi}^2$ is 18.3. The elastic and inelastic angular distribution fits for the heavy nuclei are better than those for the light nuclei.

Now, to evaluate the improvements achieved in the present coupled-channels (CC) analysis, we perform a detailed comparison with the benchmark study by Bäumer et al. [2], which reported angular distributions for deuteron elastic and inelastic scattering from ^{12}C, ^{24}Mg, and ^{58}Ni at an incident energy of E_d = 170 MeV. Their analysis was based on global optical model potentials developed by Daehnick et al. [10] and Bojowald et al. [3]. The superiority of the present approach is reflected in the reduced chi-squared (χ^2) values, which provide a quantitative measure of the fit quality. At E_d = 170 MeV, we achieved the following improvements:

- ^{12}C: χ^2 reduced from approximately 600 (using DC/BC fits) to 76,
- ^{24}Mg: χ^2 reduced from around 700 to 128,
- ^{58}Ni: χ^2 decreased from nearly 100 to 42.

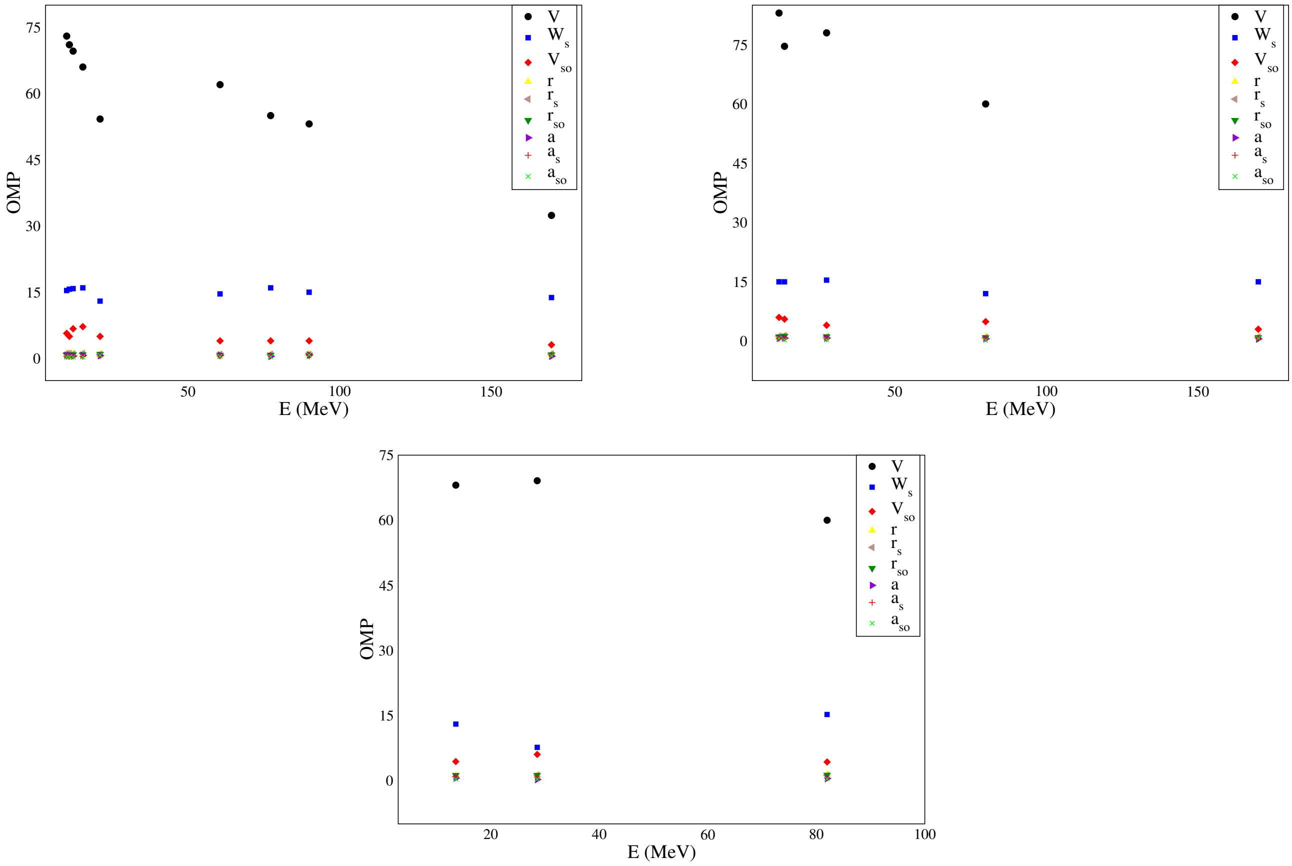

Figure 8. (Color online) The variations of the optical potential depths as a function of incident energy for ^{24}Mg (left), ^{58}Ni (right), and ^{120}Sn (bottom).

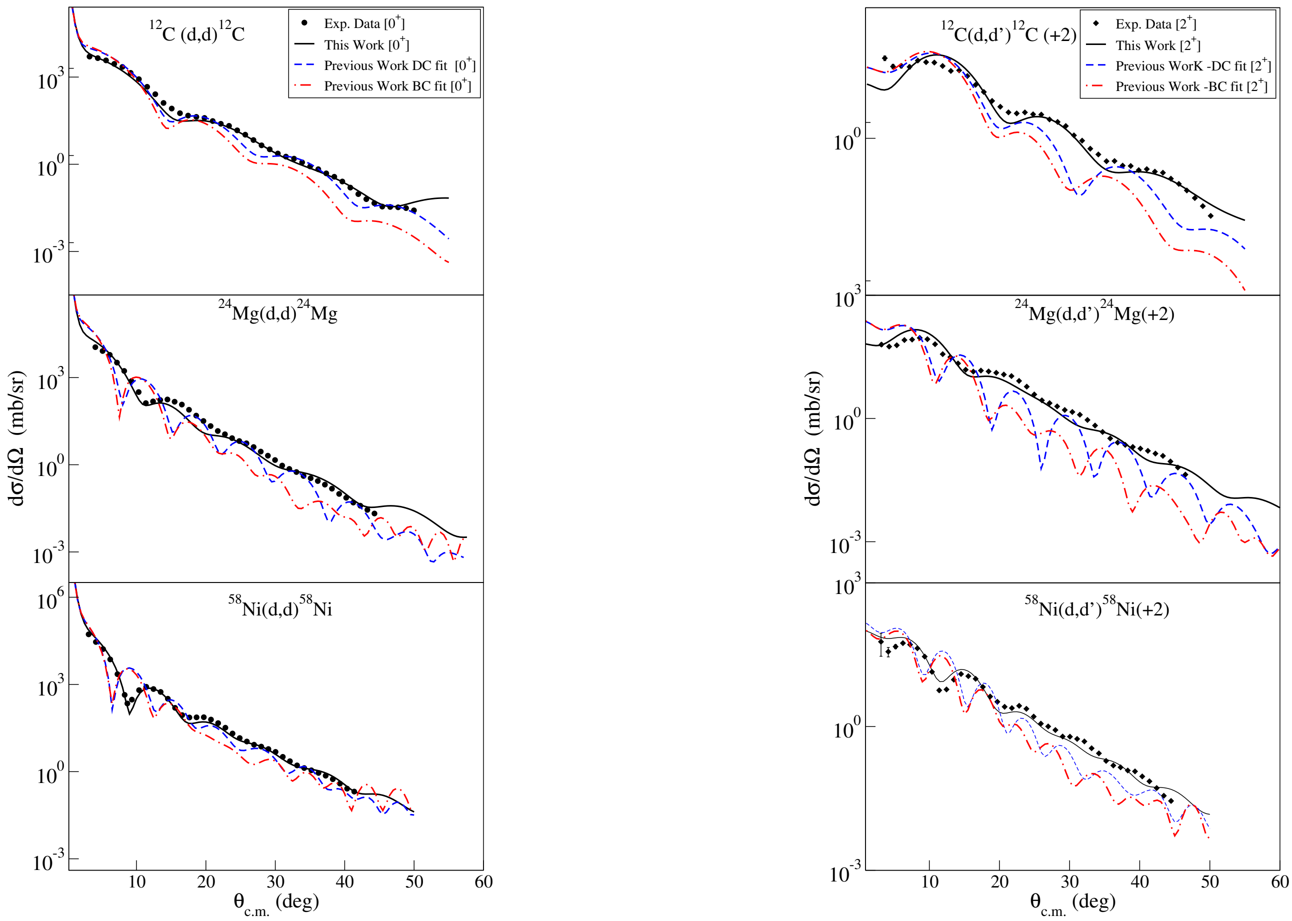

Figure 9. (Color online) Coupled channels analysis of deuteron elastic (0^+) and inelastic (2^+) scattering on ^{12}C, ^{24}Mg, and ^{58}Ni at E_d = 170 MeV. Present results (black) are compared with previous DC (blue) and BC (red) fits. The improved agreement with experiment highlights the strength of the current coupled channels approach.

5. CONCLUSIONS

In this work, we employed the coupled-channels analysis to study the deuteron-nucleus elastic and inelastic scattering processes corresponding to light and heavy nuclei in the atomic mass region from ^{6}Li to ^{208}Pb and incident energies ranging from 9.9 to 270 MeV range. The FRESCO code was used to solve the coupled partial-wave equations for a rotational nucleus. Best optical potential fit parameters were obtained for the elastic angular distribution data, in addition to simultaneous fits to the angular distributions corresponding to the most important inelastic excitations.

For light nuclei, when the elastic channel was coupled to inelastic excitations, the angular distribution fits were in excellent agreement with the experimental data as shown in Figs. (1) and (2). The variations in optical potential parameters with energy are reduced, the optical potential fit parameters for ^{6}Li and ^{12}C show lower variations with incident energy in the elastic and inelastic scattering cases.

For heavy nuclei, when coupling the ground state with the most important inelastic excitation channels the differential cross-section fits were in excellent agreement with the experimental data for the ^{24}Mg, ^{58}Ni, ^{120}Sn, and ^{208}Pb nuclei, as shown in Figures (4) to (7). We found that the optical potential fit parameters for heavy nuclei exhibit reduced variations with incident energy as shown in Tables (5) to (9). The potential parameters show smaller energy dependence in the elastic and inelastic scattering.

The main goal of our study has been to test the effect of coupled-channels analysis on the energy variation of the optical potential parameters. We found that the variations of the parameters for light and heavy nuclei are reduced when coupling is taken into account as shown in Figures (3) and (8) for the light and heavy nuclei, respectively. Therefore, we stress the following conclusions:

- The real central potential V decreases with increasing incident energy, when inelastic excitations are taken into account.
- The energy variations of the surface absorption depth W_s are more stable for the channel coupling scheme. This is so, since the imaginary part is responsible for the removal of particles from the elastic channel. Coupled channel analysis takes into account part of the removed flux explicitly. Therefore, the strength W_s of the absorption term naturally decreases.
- The real part of the spin-orbit potential V_{so} is almost constant as a function of incident energy for the light and heavy nuclei. We found that the value of V_{so} is around 4.0 MeV when the elastic channel is coupled to inelastic open excitations.

  In previous studies, the value of V_{so} was fixed at 3.55 MeV [1], V_{so} = 3.703 [20], V_{so} = 6.0 [3], and V_{so}=5.5 [10].
- The variations of the geometric parameters are highly stable when channel coupling is taken into account.

  The results demonstrate that the inclusion of inelastic couplings to collective excited states significantly improves both the physical realism and statistical quality of the fits. For example, at E_d = 170 MeV, the reduced chi-squared values for ^{12}C, ^{24}Mg, and ^{58}Ni were reduced from 600, 700, and 100, respectively, in global optical model fits to 76, 128, and 42 using our fully coupled approach. These improvements were observed not only in the forward-angle region but also in the backward-angle domain, where collective effects and interference patterns are most pronounced.

Finally, compared with previous studies, particularly the widely cited work by Bäumer et al., our approach shows clear improvements. While Bäumer's fits using global optical models and minimal coupling captured general angular trends, they suffered from large χ^2 values and poor agreement at large scattering angles. In contrast, our CC analysis with structure-informed deformation parameters and fully optimized optical potentials, yields significantly better agreement with data and enhanced physical interpretability.

In summary, the channel coupling analysis has been shown to reduce the variations of the optical parameters with energy.

ORCID

Waleed Saleh Alrayashi, https://orcid.org/0009-0009-6440-8332

REFERENCES

[1] H. An, and C. Cai, Phys. Rev. C, **73**, 054605 (2006). https://doi.org/10.1103/PhysRevC.73.054605

[2] C. Bäumer, *et al.*, Phys. Rev. C, **63**, 037601 (2001). https://doi.org/10.1103/PhysRevC.63.037601

[3] J. Bojowald, *et al.*, Phys. Rev. C, **38**, 1153 (1988). https://doi.org/10.1103/PhysRevC.38.1153

[4] A. Bonaccorso, and R.J. Charity, Phys. Rev. C, **89**, 024619 (2014). https://doi.org/10.1103/PhysRevC.89.024619

[5] B. Buck, Phys. Rev. **130**, 712 (1963). https://doi.org/10.1103/PhysRev.130.712

[6] E. Cereda, *et al.*, Phys. Rev. C, **26**, 1941 (1982). https://doi.org/10.1103/PhysRevC.26.1941

[7] D.M. Chase, L. Wilets, and A.R. Edmonds, Phys. Rev. **110**, 1080 (1958). https://doi.org/10.1103/PhysRev.110.1080

[8] S. Chiba, *et al.*, J. Nucl. Sci. Technol. **44**, 838 (2007). https://doi.org/10.1080/18811248.2007.9711356

[9] S. Cwiok, *et al.*, Comput. Phys. Commun. **46**, 379 (1987). https://doi.org/10.1016/0010-4655(87)90093-2

[10] W.W. Daehnick, J.D. Childs, and Z. Vrcelj, Phys. Rev. C, **21**, 2253 (1980). https://doi.org/10.1103/PhysRevC.21.2253

[11] H. Feshbach, Ann. Phys. **5**, 357 (1958). https://doi.org/10.1016/0003-4916(58)90007-1

[12] H. Feshbach, C.E. Porter, and V.F. Weisskopf, Phys. Rev. **96**, 448 (1954). https://doi.org/10.1103/PhysRev.96.448

[13] R.W. Finlay, *et al.*, Phys. Rev. C, **30**, 796 (1984). https://doi.org/10.1103/PhysRevC.30.796

[14] P. Fraser, *et al.*, Eur. Phys. J. A, **35**, 69 (2008). https://doi.org/10.1140/epja/i2007-10524-1

[15] M.P. Fricke, and G.R. Satchler, Phys. Rev. **139**, B567 (1965). https://doi.org/10.1103/PhysRev.139.B567

[16] M.P. Fricke, *et al.*, Phys. Rev. **156**, 1207 (1967). https://doi.org/10.1103/PhysRev.156.1207

[17] G.H. Rawitscher, Nucl. Phys. A, **475**, 519 (1987). https://doi.org/10.1016/0375-9474(87)90076-5

[18] L.J.B. Goldfarb, Nucl. Phys. **7**, 622 (1958). https://doi.org/10.1016/0029-5582(58)90105-1

[19] L. Grodzins, Phys. Lett. **2**, 88 (1962). https://doi.org/10.1016/0031-9163(62)90138-0

[20] Y. Han, Y. Shi, and Q. Shen, Phys. Rev. C, **74**, 044615 (2006). https://doi.org/10.1103/PhysRevC.74.044615

[21] G. Haouat, *et al.*, Phys. Rev. C, **30**, 1795 (1984). https://doi.org/10.1103/PhysRevC.30.1795

[22] I.N. Ghabar, and M.I. Jaghoub, Phys. Rev. C, **91**, 064308 (2015). https://doi.org/10.1103/PhysRevC.91.064308

[23] M.I. Jaghoub, *et al.*, Can. J. Phys. **100**, 309 (2022). https://doi.org/10.1139/cjp-2021-0380

[24] A.J. Koning, and J.P. Delaroche, Nucl. Phys. A, **713**, 231 (2003). https://doi.org/10.1016/S0375-9474(02)01321-0

[25] A. Korff, *et al.*, Phys. Rev. C, **70**, 067601 (2004). https://doi.org/10.1103/PhysRevC.70.067601

[26] M.I. Jaghoub, A.E. Lovell, and F.M. Nunes, Phys. Rev. C, **98**, 024609 (2018). https://doi.org/10.1103/PhysRevC.98.024609

[27] M.I. Jaghoub, and G.H. Rawitscher, Phys. Rev. C, **84**, 034618 (2011). https://doi.org/10.1103/PhysRevC.84.034618

[28] M.I. Jaghoub, and G.H. Rawitscher, Phys. Rev. C, **85**, 024608 (2012). https://doi.org/10.1103/PhysRevC.85.024608

[29] F. Perey, and B. Buck, Nucl. Phys. **32**, 353 (1962). https://doi.org/10.1016/0029-5582(62)90270-0

[30] S. Raman, C.W. Nestor Jr., and P. Tikkanen, At. Data Nucl. Data Tables **78**, 1 (2001). https://doi.org/10.1006/adnd.2001.0858

[31] S. Raman, *et al.*, Phys. Rev. C, **43**, 556 (1991). https://doi.org/10.1103/PhysRevC.43.556

[32] S. Raman, and C.W. Nestor Jr., Phys. Rev. C, **37**, 805 (1988). https://doi.org/10.1103/PhysRevC.37.805

[33] G.H. Rawitscher, and D. Lukaszek, Phys. Rev. C, **69**, 044608 (2004). https://doi.org/10.1103/PhysRevC.69.044608

[34] S. Alameer, M.I. Jaghoub, and I. Ghabar, J. Phys. G: Nucl. Part. Phys. **49**, 015106 (2022). https://doi.org/10.1088/1361-6471/ac3e3b

[35] W.S. Al-Rayashi, and M.I. Jaghoub, Phys. Rev. C, **93**, 064311 (2016). https://doi.org/10.1103/PhysRevC.93.064311

[36] I.J. Thompson, Comput. Phys. Rep. **7**, 167 (1988). https://doi.org/10.1016/0167-7977(88)90005-2

[37] T. Tamura, Rev. Mod. Phys. **37**, 679 (1965). https://doi.org/10.1103/RevModPhys.37.679

[38] V.M. Strutinsky, Nucl. Phys. A, **95**, 420 (1967). https://doi.org/10.1016/0375-9474(67)90510-6

[39] G.M. Crawley, and G.T. Garvey, Phys. Rev. **160**, 981 (1967). https://doi.org/10.1103/PhysRev.160.981

[40] R.H. Spear, Phys. Rep. **73**, 369 (1981). https://doi.org/10.1016/0370-1573(81)90059-4

[41] D. Woods, and D.S. Saxon, Diffuse Surface Optical Model for Nucleon-Nuclei Scattering, Phys. Rev. **95**, 577 (1954). https://doi.org/10.1103/PhysRev.95.577

[42] A. Bohr, and B.R. Mottelson, *Kgl. Danske Videnskab. Selskab, Mat. Fys. Medd.* **27**, No. 16 (1953).

[43] A. Bohr, and B.R. Mottelson, *Nuclear Structure*, Vol. I (W. A. Benjamin, New York, 1969).

[44] I.J. Thompson, and F.M. Nunes, *Nuclear Reactions for Astrophysics* (Cambridge University Press, Cambridge, 2009).

[45] A.S. Green, *The Nuclear Independent Particle Model: The Shell and Optical Models* (Academic Press, New York, 1968).

[46] H. Feshbach, *Theoretical Nuclear Physics: Nuclear Reactions* (John Wiley and Sons, 1982).

[47] J.M. Eisenberg, and W. Greiner, *Nuclear Models, Vol. I* (North-Holland, Amsterdam, 1970).

[48] A.J. Koning, S. Hilaire, and M. Duijvestijn, in *Proc. Int. Conf. Nucl. Data for Science and Technology*, Nice, France, 2007 (EDP Sciences, 2008), p. 211. https://doi.org/10.1051/ndata:07767

[49] EXFOR — Experimental Nuclear Reaction Data, IAEA. https://www-nds.iaea.org/exfor/

[50] CINDA — Computer Index of Nuclear Reaction Data, IAEA. https://www-nds.iaea.org/exfor/cinda.htm

[51] R.L. Walter, and R.M. Drisko, Phys. Rev. **124**, 832 (1961). https://doi.org/10.1103/PhysRev.124.832

[52] S.M. Smith, and D.A. Goldberg, Phys. Rev. **129**, 2690 (1963). https://doi.org/10.1103/PhysRev.129.2690

[53] D.A. Goldberg, and S.M. Smith, Phys. Rev. **129**, 2683 (1963). https://doi.org/10.1103/PhysRev.129.2683

[54] Y. Sakuragi, M. Yahiro, and M. Kamimura, Phys. Rev. C, **35**, 2161 (1987). https://doi.org/10.1103/PhysRevC.35.2161

[55] O. Aspelund, J.S. Lilley, and J.D. Hemingway, Nucl. Phys. A, **253**, 263 (1975). https://doi.org/10.1016/0375-9474(75)90263-5

[56] Y. Satou, *et al.*, Phys. Rev. C, **65**, 054602 (2002). https://doi.org/10.1103/PhysRevC.65.054602

[57] Y. Satou, *et al.*, Phys. Lett. B, **549**, 307 (2002). https://doi.org/10.1016/S0370-2693(02)02957-X

[58] M. Beiner, *et al.*, Nucl. Phys. A, **238**, 29 (1975). https://doi.org/10.1016/0375-9474(75)90378-7

[59] S. Hinds, *et al.*, Nucl. Phys. A, **113**, 314 (1968). https://doi.org/10.1016/0375-9474(68)90574-0

[60] M.A. Franey, R.L. Boudrie, and B.D. Anderson, Phys. Rev. C, **29**, 1118 (1984). https://doi.org/10.1103/PhysRevC.29.1118

АНАЛІЗ ЗВ'ЯЗАНИХ КАНАЛІВ ТА ВИЛУЧЕННЯ ПОТЕНЦІАЛУ ОПТИЧНОЇ МОДЕЛІ ДЛЯ РОЗСІЮВАННЯ ДЕЙТРОНІВ ВІД ^{6}Li ДО ^{208}Pb

Валід Салех Альраяші
Кафедра науки, факультет освіти, Університет Сани, Сана, Ємен

Пружне та непружне розсіювання дейтрон-ядро від ^{6}Li до ^{208}Pb було досліджено для енергій падіння від 9,9 до 270 МеВ. Головною метою цієї роботи є вивчення впливу зв'язку основного стану ядра з непружними каналами збудження на енергетичну залежність параметрів оптичного модельного потенціалу (ОМП). Використовуючи коди FRESCO та SFRESCO, ми явно пов'язали пружний канал з низько розташованими колективними станами та вилучили параметри ОМП шляхом мінімізації χ^2. Найкращі параметри оптичної моделі були отримані для даних пружного та непружного кутового розподілу. Наші апроксимації кутового розподілу пружності та непружності демонструють чудову відповідність з експериментальними даними, оскільки більше одного набору параметрів потенціалу може відтворити задані дані кутового розподілу. Коли основний стан був пов'язаний з найважливішими непружними каналами збудження, енергетична залежність параметрів ОМР зменшилася. Це найбільш очевидно для параметрів оптичної моделі, значення яких стало майже постійним, коли розглядався зв'язок каналів.

Ключові слова: *реакції зв'язаних каналів; дейтрон; пружне розсіювання; непружне розсіювання; параметри потенціалу оптичної моделі; диференціальний поперечний переріз*